RSC Advances

PAPER

View Article Online
View Journal | View Issue

Cite this: *RSC Adv.*, 2022, **12**, 28560

Received 7th September 2022
Accepted 20th September 2022

DOI: 10.1039/d2ra05632a

rsc.li/rsc-advances

Single-factor analysis of Ni–B–AC-catalyzed β-pinene hydrogenation based on hierarchical analysis†

Qiao Deng, Lihong Jiang,* Yu Yang and Yan Yu

In the choice of catalysts for the hydrogenation of pinene, nickel-based catalysts show intriguing activity. Here, a Ni–B catalyst supported on activated carbon with Ni as an active component was synthesized by the titration reduction co-impregnation method. The mechanism of such heterogeneous systems has not yet been articulated, and the industrial applications of the potassium borohydride reduction of nickel-based catalysts are limited by their easy agglomeration and poor stability. The materials were analyzed by hierarchical and DFT studies, *in situ* XPS, BET, XRD, and SEM, which provided insights into the kind of signals in Ni^{2+} reduction to Ni^0. The hierarchical analysis indicated that Ni/AC (0.4876) and reaction pressure (0.6066) influenced the catalyst preparation and process efficiency changes, respectively. Activated carbon was shown to provide a favorable basis for the stability of the Ni–B activity. In addition, the hierarchical analysis method provides new insights into the data analysis for chemical experiments.

1. Introduction

With the continuous development of new synthetic substances in recent years, *cis*-pinane is now being engineered to manufacture a wide range of chemicals, pesticides, flavorings, drugs, and fuels,[1–4] which is accessible by the transformation of α-pinene and β-pinene under hydrogen partial pressure. The preparation of *cis*-pinane presents a lucrative economy, well-balanced structure, and has profound utility to research as a key intermediate.[5–7] Turpentine is dominated by α-pinene and β-pinene, and consequently, the further hydrogenation of pinene is favored and requires an enhanced hydrogenation ability of a heterogeneous catalyst. Here, heterogeneous catalysts offer advantages over single metals in terms of their post-use recycling and reuse.[8,9] Other than the existing published catalysts, a latent avenue to boost the selectivity and conversion of the process is to bring in an efficient and stable catalyst carrier,[10–13] and again, activated carbon-loaded rhodium,[14,15] platinum,[16,17] and rubidium[18,19] are among the more studied catalysts, showing equally fine results. Nevertheless, hydrogenation catalysts, such as Ni–B, can affect the process efficiency. For this reason, the use of stable and efficient hydrogenation catalysts for the preparation of *cis*-pinane allows for high quality to be achieved. Overall, the biggest problems in catalyst production are the production cost, reaction efficiency, and the stability of the catalyst itself.[20–22] The study of hydrogenation catalysts is thus of great practical importance.

The choice of catalyst should be predicated on high catalyst efficiency, stable catalyst performance, and a steady catalyst structure.[23–25] Furthermore, if the catalyst consists of an enriched pore volume and pore size,[26–28] there would be more active ingredient adsorption sites, which would help to improve the overall performance of the catalyst. For the sake of investigating the efficiency of pinene catalysts, including the catalyst and catalyst carrier, to understand the active ingredient sites, it was necessary to explore and develop new catalysts for hydrogenation. Furthermore, Ni–B catalysts have some key limitations, including feeble stability, arbitrary oxidation, and active site deficiency, and hence, a stable matrix material needs to be selected to overcome these disadvantages.[29,30]

In the present study, a Ni–B–AC catalyst was used for the first time for the hydrogenation of β-pinene. The single factors affecting the catalyst preparation were experimentally investigated and the weights of each factor were determined using hierarchical analysis, followed by an analysis of the catalysts by BET, XRD, and XPS, and verification of the morphology of the catalysts by density functional theory (DFT) calculations performed in Gaussian 16.

2. Materials and methods

2.1 Catalyst preparation and hydrogenation process

The catalyst was prepared by a static reduction in a low-temperature alcohol bath. Activated carbon (1.4 g), $NiCl_6 \cdot 6H_2O$ (0.9 g, 0.2 mol L^{-1}), and 50.00 mL of ethanol solution were stirred

---

Faculty of Chemical Engineering, Kunming University of Science and Technology, No. 727 Jingming South Road, China. E-mail: jlh65@163.com

† Electronic supplementary information (ESI) available. See https://doi.org/10.1039/d2ra05632a

in a three-necked round-bottom flask under nitrogen protection and placed in an alcohol bath 0 °C, with magnetic stirring at speed 7 for 30 min. Next, KBH_4 (1.00 g, 0.3 mol L^{-1}) solution was prepared, and 0.2 mol L^{-1} sodium hydroxide was added to adjust the pH to 13. The KBH_4 solution was then dropped into the above three-necked round-bottom flask through an infusion tube and a one-pot reaction occurred for 4 h. After completion of the reaction, repeated washing steps with water were performed to remove the solution, and a final wash with ethanol was used to remove the water. The remaining solid catalyst in the filter paper was dried in a vacuum drying oven for 6 h at 60 °C.

To a high-pressure vessel equipped with a thermocouple was added β-pinene (10 g) and the catalysts (5 wt%) and ethanol solvent (10 mL). The overall reaction was carried out at 130 °C for 2 h, and at 3.0 MPa and 800 r per min. After the hydrogenation reaction was complete, the reactor was naturally cooled down to room temperature, and the reaction solution was filtered to remove the catalysts, and the organic liquid to be tested was diluted with ethanol.

2.2 β-Pinene test conditions

The single-factor values affecting the catalysts were determined by gas chromatography (GC 2014). The test conditions for the GC were: DB-5 capillary column (size 30 m × 0.32 mm × 0.5 m), flame ionization detector (FID), high purity nitrogen as the carrier gas, high purity hydrogen as the fuel gas, air as the auxiliary gas, gasification chamber temperature of 250 °C, detector temperature of 250 °C, pressure of 62 KPa, split ratio of 1 : 50, injection volume of 0.5 μL, and temperature program comprising $75\ ℃ \xrightarrow[10\ \text{min}]{1.5\ ℃} 90\ ℃ \xrightarrow[3\ \text{min}]{20\ ℃} 150\ ℃$. The experimental data could be well analyzed by the area normalization method, which was normalized by dividing the individual peak area by the total peak area of all peaks for that sample.

2.3 Catalyst characterization

The materials were characterized by N_2 adsorption–desorption isotherms, XRD, XPS, and SEM. The specific surface area was measured using a NOVA 4200e automatic system with a degassing temperature of 80 °C, degassing time of 12 h, and an adsorbent of N_2. XPS was performed on an Escalab 250 Xi-phi-Ves probe 5000 Thermo-Fischer (USA) instrument, employing Al Kα radiation (hv = 1486.6 eV, 14.6 kV, 13.5 mA, 20 cycles), with charge correction performed by passing energy of 20 eV in steps of 0.1 eV, using the binding energy of C 1s = 284.8 eV as the energy standard. X-Ray diffractometer (XRD) measurements were carried out on a Nishiko Ltd model D/max2200 system (Japan), using Cu-K radiation and scanning powder samples at a wide angle of 10° per min in the range 5°–90°. DFT-assisted Ni-B calculations were performed using Gaussian 16 and Multiwfn 3.8 software.

2.4 Analysis methods

2.4.1 Preparation of the catalysts and processing the experimental data for the hydrogenation processes.

$$\text{Conversion rate} = \frac{\text{Amount of } \beta - \text{pinene in turpentine} - \text{amount of residual pinene in the product}}{\text{Amount of } \beta - \text{pinene in turpentine}}$$

$$\text{Selectivity} = \frac{\left(\dfrac{\text{cis} - \text{pinane}}{138.25}\right)}{\left(\dfrac{(\text{Amount of } \beta - \text{pinene in the raw material} - \text{Amount of } \beta - \text{pinene in the product})}{136.23}\right)}$$

2.4.2 Data reliability analysis methods: the hierarchical analysis process (AHP). Hierarchical analysis is an analytical approach for making decisions on a number of complex and single-factor problems. It is chiefly applied for the quantitative analysis of qualitative indicators by constructing a multi-level evaluation index system, which is suitable for problems that are difficult to analyze completely quantitatively. The method was used here for the single-factor analysis of the catalyst preparation and for parametric analysis of the hydrogenation process, using the yield as a judgment indicator for the analysis. The analysis steps were as follows (Fig. 1).

3. Results and discussion

3.1 Single-factor examination of the catalyst preparation

During the preparation of the Ni–B–AC catalysts, the stability of the catalysts slightly varied based on the preparation

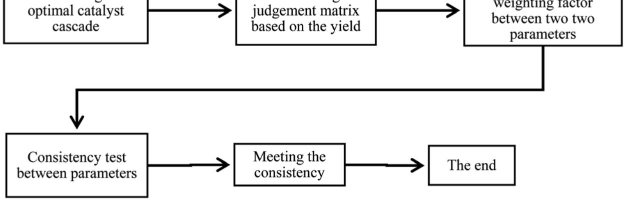

Fig. 1 AHP analysis step-by-step process.

conditions.[31,32] The optimum preparation conditions were determined by varying the pH value, reaction time, drop acceleration, Ni/AC mass ratio, and the ratio of the reducing agent to the active component Ni. The highest β-pinene conversion and pinane selectivity of the Ni–B–AC catalysts occurred at 130 °C, 3.0 MPa, 5 wt%, 800 r per min, and 120 min. The following data are from a study of the conditions under which the catalysts were prepared.

The study of the optimum pH of the catalyst preparation process is shown in Fig. 2a. In a weakly alkaline environment, the pH contributed to the formation of Ni–B–AC.[21,33,34] The pH range was 9–14. When the pH was minimal, the whole system may be free of Ni^{2+}. As the pH increased, the reduction efficiency of Ni^{2+} increased, with a consequent increase in the conversion and selectivity. At pH 13, as the alkalinity increases, Ni^{2+} was reduced to Ni^0, contributing to Ni^0 loading on the activated carbon. At this point the conversion and selectivity reached a maximum.[35,36] The reduction time of the catalysts prepared by impregnation was also a pivotal factor, whereby when the stirring rate and alcohol bath temperature were fixed, the conversion and selectivity of the impregnation reaction changed gradually as the reaction time increased or decreased. The study of the reaction times during the catalyst preparation is shown in Fig. 2b and c. When the first drop of reducing agent was dropped into the nickel-containing solution, the reaction was violent and produced a significant amount of bubbles, with bubbles continuing to be generated for 20 min. When the reaction time was more than 4 h, the conversion and selectivity of β-pinene hydrogenation decreased. The drop in acceleration rate of the reducing agent was crucial for the preparation of the Ni–B activated carbon, whereby too fast or uneven stirring was not conducive to the reduction of nickel hexachloride H_2O, while too slow had issues reaching saturation, and so 50 drops per min was found to be the optimal rate. It has been reported that the reduction of Ni^0 can reach saturation with a rapid rate of decline, at which point some unreacted Ni may be encapsulated within Ni^0.[37,38]

The stability of the loaded catalysts was also related to the properties of the loaded substrate, pore volume, pore size, and specific surface area.[39–42] It can be seen from the analysis of Fig. 2d and e, at a mass ratio of 1 : 4, the conversion and selectivity may be low due to the small amount of Ni loaded on the activated carbon; whereas when at a mass ratio of 1 : 7, both conversion and selectivity reached a maximum. The active component Ni in the catalyst preparation was closely related to the addition of the reducing agent B, wherein the best ratio of Ni to B was 1 : 4. Whereas, as the ratio of Ni to B increased, saturation, encapsulation, and the agglomeration of Ni may occur during the dropwise addition of the reductant B, resulting in a gradual decrease or even leveling off of the selectivity and conversion.[21,43,44,45]

3.2 Exploring the hydrogenation process

The hydrogenation catalysts were prepared under the optimum preparation conditions described above. The effects of the stirring speed, temperature, pressure, and catalyst amount on the hydrogenation process were investigated. The

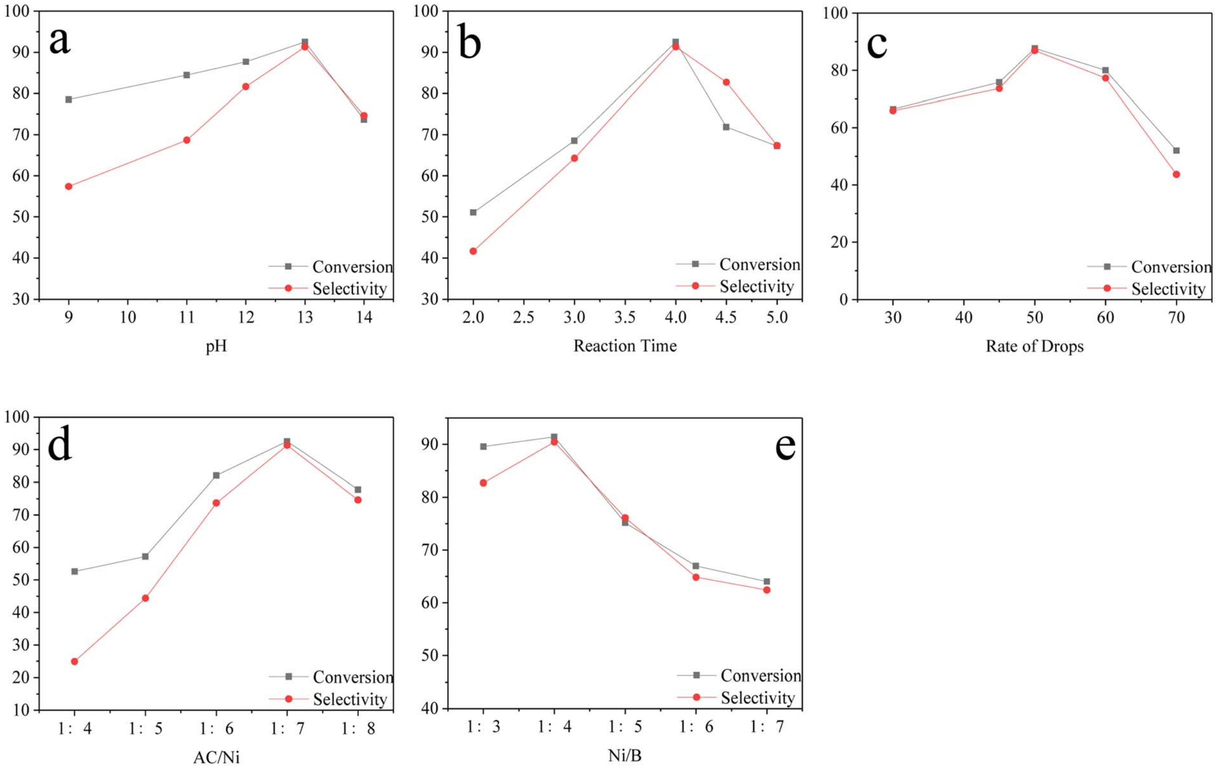

Fig. 2 Determination of the single factors affecting the catalyst preparation.

fixed factors were 2 h and 10 g β-pinene, with the range of catalyst amount set at 3–7 wt%, temperature 90–140 °C, pressure of 2.0–5.0 MPa, and stirring speeds of 500–850 r per min. The following data were examined for the catalyst preparation conditions.

As can be seen from Fig. 3a, there was a trend toward the increasing conversion and selectivity of the hydrogenation reaction with increasing the magnetic rotor stirring speed. At speeds of 500–750 r per min, the reaction was probably designed to eliminate external diffusion, while at a speed of 800 r per min, the material was stirred to push toward the kettle wall, leading to a reduced catalyst amount. As can be seen from Fig. 3b, as the amount of catalyst increased, the conversion tended to become more stable and the selectivity gradually increased, with the optimum mass ratio being 5 wt%. The reaction pressure also played a major role in the catalytic reaction. As can be seen from Fig. 3c, as the pressure increased to 3.0 MPa, there was an inflection point for the conversion and selectivity, with a decreasing trend and an optimum reaction pressure of 3.0 MPa. Temperature also promoted the catalytic reaction to be carried out. Hydrogenation belongs to an exothermic reaction, and so the conversion and selectivity incrementally increased as the temperature increased, as can be seen from Fig. 3d, and then sluggishly decreased when the temperature rose to 120 °C. These changes may be due to the effect of the partial catalysts properties of the kettle at high temperature.[46,47,48]

3.3 Hierarchical analysis (AHP) of the data for each factor for β-pinene hydrogenation

3.3.1 Single-factor analysis affecting the catalyst preparation. Hierarchical analysis was carried out to analyze the experimental data on the single factors.[49–52] The stratification structure is shown in Fig. 4 and the main objective was to obtain the best single factor. Five indicators: pH of the reducing agent, reaction time of the catalyst preparation, drop in acceleration of the reducing agent, and Ni/AC and Ni/B ratios were used as the standard layers, with the individualized next-level indicators of each factor used as the sub-standard layers. The differences in β-pinene hydrogenation yields were used to form a judgment matrix on a scale from 1–9 and the results were analyzed.[53] The consistency index of the intermediate elements ($0.0202 \neq 0$) and the consistency ratio of the five indicators ($0.0180 < 0.1$) indicated that the consistency of the judgment matrix of the intermediate elements and the inter-pair sorting results were acceptable, and the weighting coefficients obtained were reasonably valid without logical confusion.

The results covered the sub-target reductant pH concentration index ($0.0215 \neq 0$) and the concentration ratio between different gradients of pH ($0.0192 < 0.1$); the reaction time

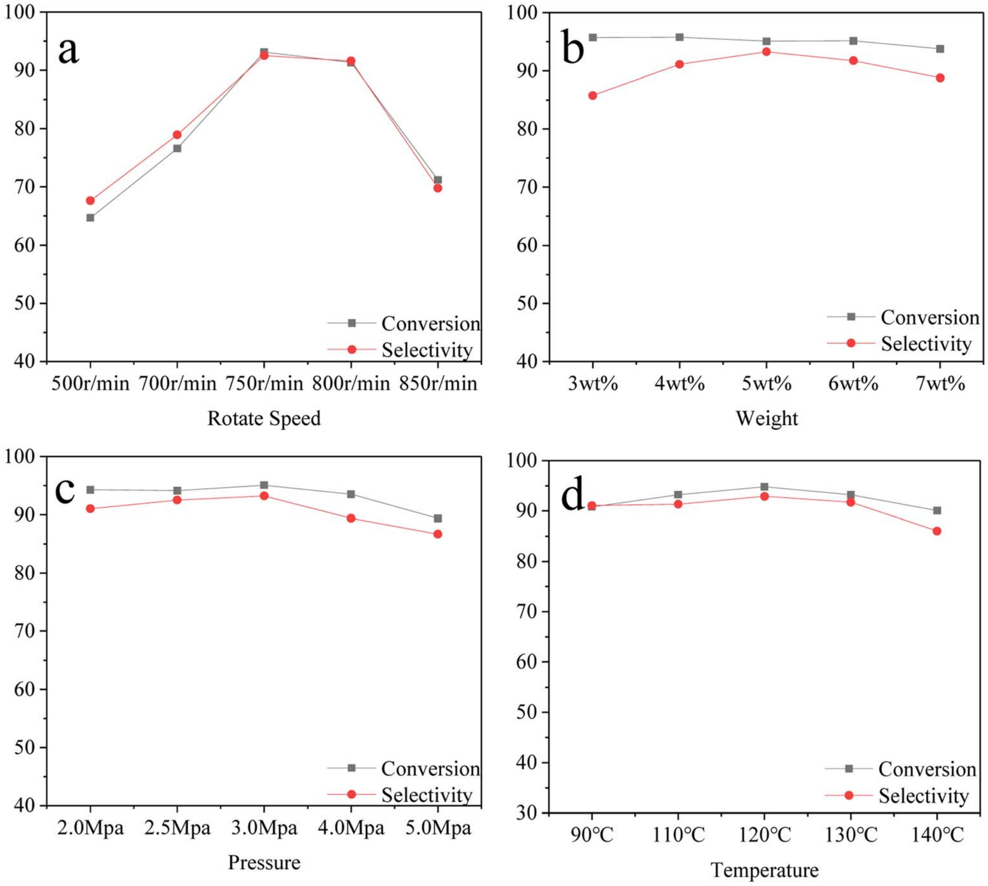

Fig. 3 Single-factor examinations of the hydrogenation process.

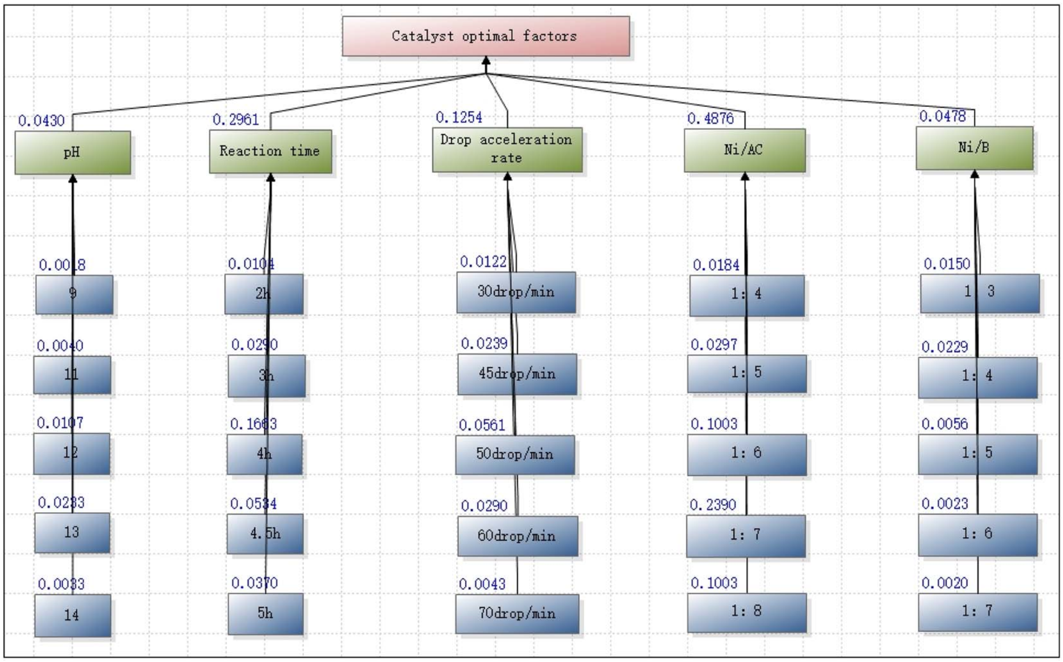

Fig. 4 Distribution of weights for each element in the catalyst preparation.

consistency index ($0.2291 \neq 0$) and the consistency ratio ($0.0511 < 0.1$); the consistency index of the drop rate ($0.0213 \neq 0$) and the consistency ratio ($0.0190 < 0.1$); the index of the mass ratio of Ni/AC ($0.0192 \neq 0$) and the consistency ratio ($0.0171 < 0.1$); and the consistency of the quantity ratio of Ni/B substances ($0.0293 \neq 0$) and each substance ($0.0262 < 0.1$). All the above factors satisfied the consistency, while the weighting factors were all reasonable and valid.

As can be seen from Fig. 4, the Ni/AC ratio (0.4876) was the most important element in the interlayer. A suitable active component Ni/AC ratio can stabilize the catalyst, which was related to the loading of the active component and the specific surface area. The index analysis further indicated the formation

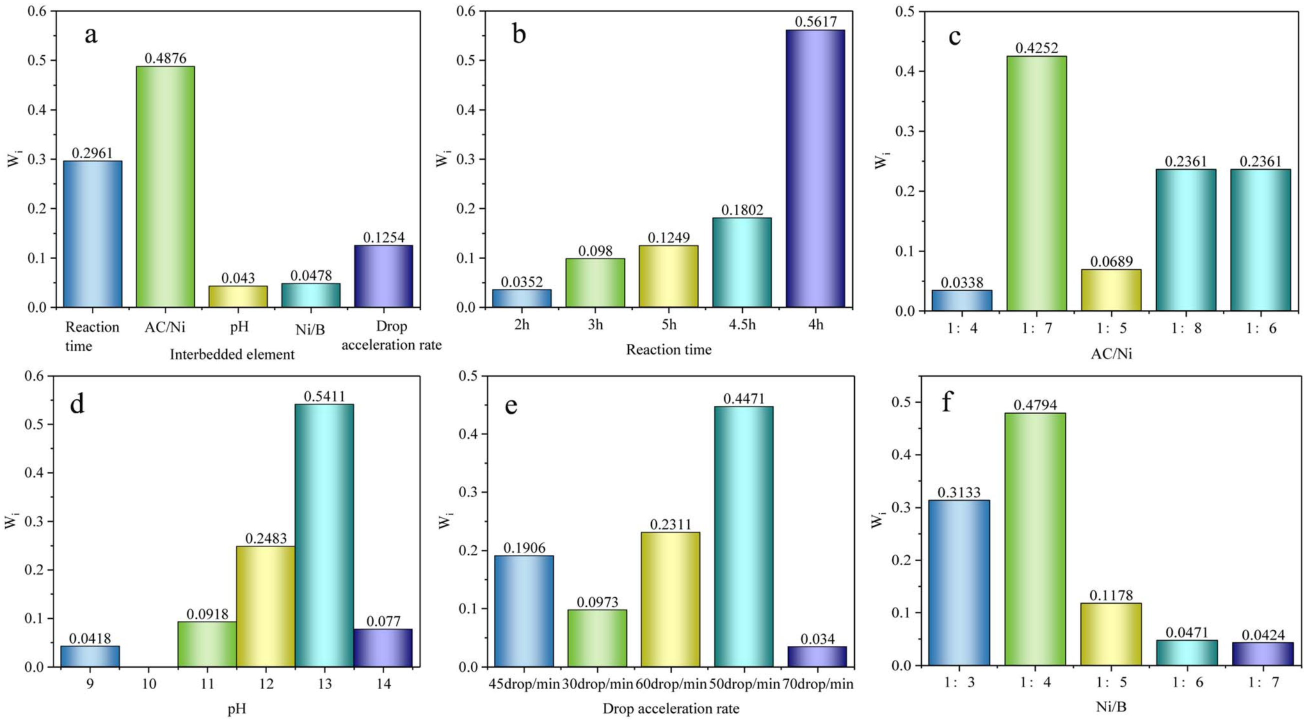

Fig. 5 Graph of the weighting ratios between the two factors of the hydrogenation process.

of Ni–B–AC-loaded catalysts and showed that the key to the catalyst preparation was to master the Ni/B and Ni/AC ratios.

As per the analysis in Fig. 5, disparate single-factor indicators showed distinct hydrogenation effects during the catalyst preparation. Fig. 5a shows the single-factor weighting ratio of Ni/AC (0.4876) with a relatively large reaction time (0.2961). Fig. 5b depicts the reaction time during the catalyst preparation, with a large proportion at 4 h (0.5617) and 4.5 h (0.1802), indicating that the yield gradually increased with time, but then gradually decreased after a certain time. Fig. 5c shows that for the Ni/AC ratio, 1 : 7 (0.4252), 1 : 8, 1 : 6 (0.2361) accounted for a large proportion of the catalyst preparation. Fig. 5d shows the pH during the catalyst preparation, with pH 13 (0.5411) and 12 (0.2483) accounting for large proportions. Fig. 5e shows the drop in acceleration rate with 50 drops per min (0.4471) and 60 drops per min (0.2311) accounting for large proportions. Fig. 5f shows that during the catalyst preparation, 1 : 4 (0.4794) and 1 : 3 (0.3133) represented relatively large Ni/B ratios. Pursuant to the data analysis, the optimal reaction time was 4 h, the Ni/AC ratio was 1 : 7, the pH was 13, the drop in rate was 50 drops per min, and the Ni/B ratio was 1 : 4, which was consistent with the results of the single-factor examination.

3.3.2 Single-factor analysis of the hydrogenation process. Hierarchical analysis was used to analyze the single-factor data from the hydrogenation process. The hierarchical structure is shown in Fig. 6. The main objective was to obtain the best single factor for the process. Four indicators, namely the stirring speed, reaction pressure, catalyst dosage, and reaction temperature, are used as criterion layers, and the individual indicators for each factor were used as sub-criteria layers. Using the differences in hydrogenation yields of β-pinene, a judgment matrix was constructed on a scale of 1–9 and the results were analyzed.

The results demonstrated the consistency index of the middle element (0.0448 ≠ 0) and the consistency ratio of the five indicators (0.0504 < 0.1); the consistency index of the sub-objective stirring speed (0.0224 ≠ 0) and the consistency ratio (0.0200 < 0.1); the consistency index of the reaction pressure (0.0312 ≠ 0) and the consistency ratio (0.0279 < 0.1); the consistency index of the catalyst amount (0.0131 ≠ 0) and the consistency ratio (0.0117 < 0.1); and the consistency index of the reaction temperature (0.0213 ≠ 0) and the consistency ratio (0.0190 < 0.1). All the above data indicate that the judgment matrix of the middle element was consistent, and that acceptable weighting coefficients were obtained that were reasonably valid without logical confusion.

As can be seen from Fig. 6, the reaction pressure (0.6066) and the amount of catalyst (0.2110) were the main factors for the intermediate layer. An appropriate pressure helps to reduce the burden of the reaction; while the importance of choosing the catalyst dosage should not be overlooked. In practical industrial applications, the catalyst dosage will be selected on the basis of low cost and large benefits to help achieving the industrial goals.

As can be seen Fig. 7a, the reaction pressure (0.6066) had the largest share and thus impact by far. Fig. 7b shows the stirring speed, with 750 r per min (0.4144) and 800 r per min (0.3936) having relatively large shares. Fig. 7c shows the reaction pressure, with 3.0 MPa (0.3496) and 2.5 MPa (0.2942) accounting for a relatively large proportion. Fig. 7d shows the amount of catalyst, with 4 wt% (0.3199) and 5 wt% (0.3075) accounting for relatively large amounts, while Fig. 7e shows the reaction temperatures, with 120 °C (0.3545) and 130 °C (0.2833) prominent. In summary, the data analysis showed that a stirring speed of 750 r per min, a reaction pressure of 3.0 MPa, a catalyst dosage of 4 wt% and a reaction temperature of 120 °C were optimal. The single-factor process experiments were highly consistent compared to each other.

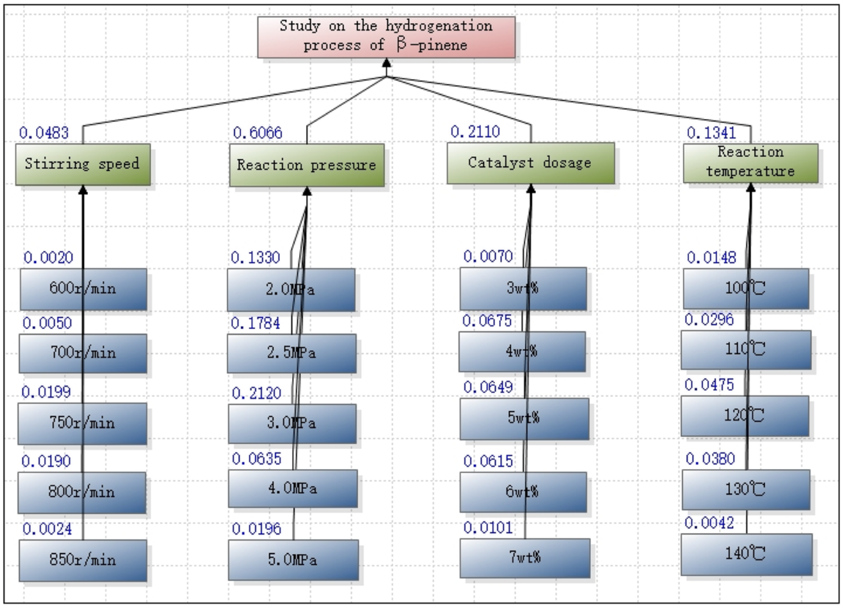

Fig. 6 Optimal conditioned hierarchical analysis diagram for the hydrogenation process.

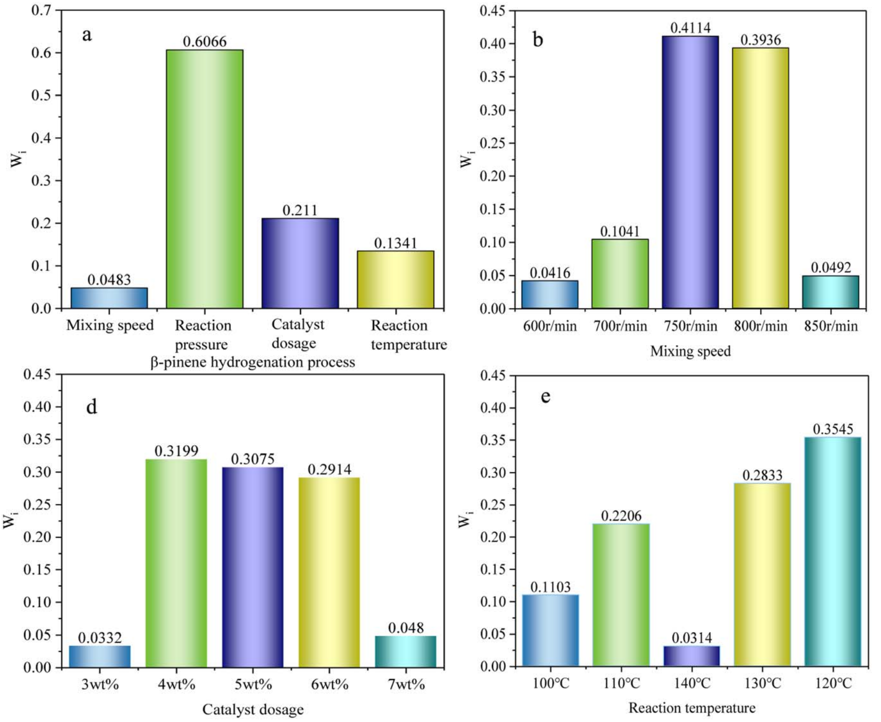

Fig. 7 Graph of the weighting ratios between two factors of the hydrogenation process.

3.4 Experimental characterization and computational verification

3.4.1 Characterization of the experimental materials. The Ni–B–AC materials were characterized by nitrogen adsorption–desorption isotherms, XRD, and XPS. The specific surface area, pore volume, and pore size of the material were analyzed by nitrogen adsorption–desorption isotherms, as shown in Fig. 8a and b. The crystalline state of the material was determined by wide-angle XRD, as shown in Fig. 8c. XPS allowed the analysis of the specific elements contained in the material, as shown in Fig. 8d.

According to the characterization data in Fig. 8a above, the specific surface area adsorption and desorption curves at different pH values were consistent with a type-IV isotherm, with a specific surface area of 719.841 $m^2 g^{-1}$ at pH 13. The pore structure in Fig. 8b shows that the pore sizes between 5 and 10 were mesoporous. The AC in Fig. 8c (XRD) is a raw material for activated carbon, as can be seen from the graphite peak at $2\theta = 28°$. A graphite peak was still present in the loaded Ni–B–AC activated carbon sample. When it was in the range of 20°–30°, at $2\theta = 45°$, both AC and Ni–B–AC showed a large diffraction peak and a small diffraction peak, indicating that the material was amorphous. Fig. 8d shows that the sample contained elements such as C, O, Ni, and B. The element O 1s in the spectrum was probably from the oxygen-containing functional group of the activated carbon loaded on the substrate with a binding energy

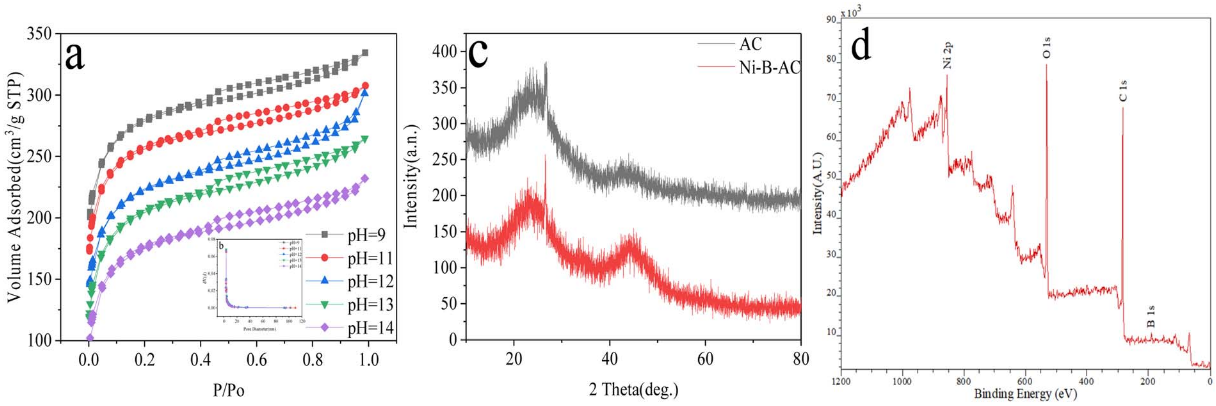

Fig. 8 Ni–B–AC-loaded catalyst: (a and b) N_2 adsorption and desorption profiles ((b) is presented as the inset), (c) wide angle XRD, (d) XPS analysis.

of 529.41 eV. The element C 1s in the figure was from the carbon-based component of the activated carbon with a binding energy of 282.35 eV. In the spectrum, the active component Ni 2p element was from $NiCl_2 \cdot 6H_2O$ with a binding energy of 857.65 eV, while B 1s was from the reducing agent KBH_4 solution, with a binding energy of 187.06 eV. The above spectra indicated that the loaded catalyst Ni–B–AC had been successfully loaded with a high specific surface area, good stability, and an abundance of active sites, which contributed to improving the catalytic activity.

3.4.2 DFT calculations of the analytical data

3.4.2.1 Calculation of the basic information. The Ni–B structure and stability were analyzed by density functional theory (DFT) in Gaussian 16[54] and Multiwfn 3.8.[55] In order to consider the effect of Ni–B, the possible configurations of the atomic clusters were optimized at the B3LYP/6-311 + g(d) level using DFT, and at the same time, the single-point energy was calculated under the 6-311++g(d) basis set, which could obtain the high-precision energy, and allow analyzing the electrostatic potential. The binding sites were observed by electrostatic potential diagrams to obtain stable monomers.[34,56]

According to Table 1 above, the basic structure of the bond lengths showed that B–B bonds could be found between the NiB_2, Ni_2B_2, and Ni_3B_2 molecules, while there were no chemical bonds between B–B in the Ni_4B_2 molecule. It could also be predicted that Ni_4B_2 clusters would form more readily than NiB_2, Ni_2B_2, and Ni_3B_2 molecules, which was consistent with the experimental results. As the number of Ni atoms increased, the

Table 1 Key lengths after the structural optimization

Molecular	Key type	Key length/Å	Key type	Key length/Å	G/hartree
NiB_2	Ni_3–B_1	1.883	B–B	1.563	−1559.136
Ni_2B_2	Ni_4–B_1	1.909	B–B	1.695	−3066.196
	Ni_4–Ni_3	2.198			
Ni_3B_2	Ni_4–B_1	1.914	B_1–B_2	1.899	−4574.543
	Ni_4–Ni_3	2.226			
	Ni_5–B_1	1.842			
	Ni_4–B_1	1.915			
	Ni_3–Ni_5	3.025			
Ni_4B_2	Ni_4–B_6	1.952	—	—	−6082.889
	Ni_4–Ni_3	2.236			

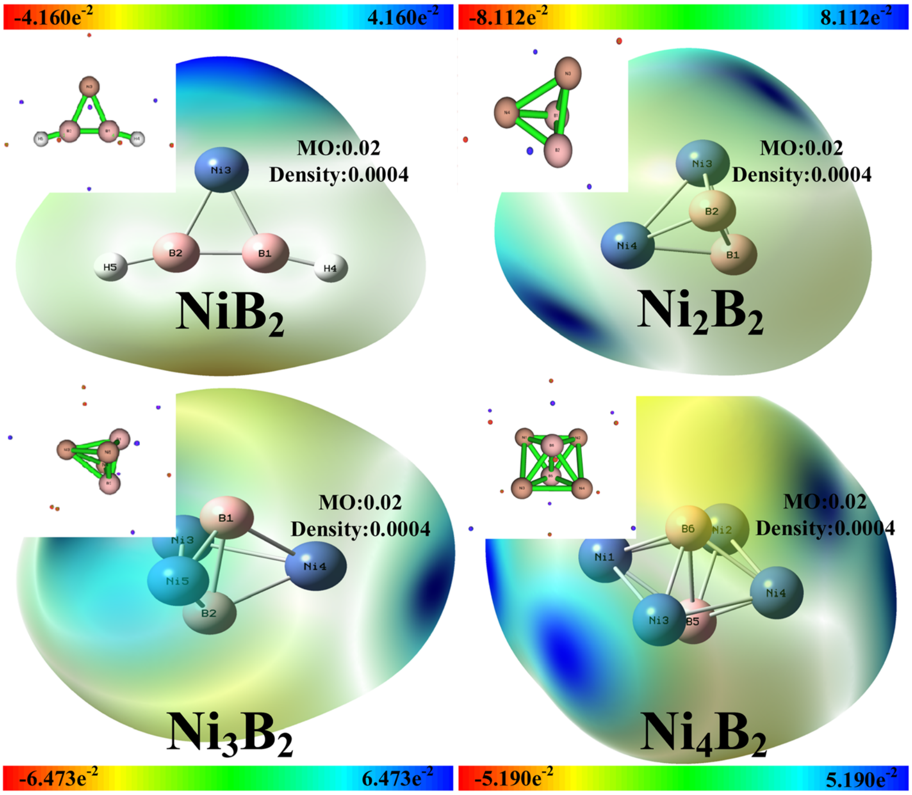

Fig. 9 Electrostatic potential diagrams for NiB_2, Ni_2B_2, Ni_3B_2, and Ni_4B_2.

Table 2 Molecular charges

Molecular	Electropositive sites (charge)	Electronegative sites (charge)	Electrostatic potential
NiB_2	$Ni_3(0.012)$	$B_1(-0.047)$ $H_4(-0.041)$	$-4.160e^{-2}$–4.160×10^{-2}
Ni_2B_2	$Ni_3(0.014)$	$B_2(-0.014)$	$-8.112e^{-2}$–8.112×10^{-2}
Ni_3B_2	$B_1(0.117)$	$Ni_3(-0.083)$ $Ni_5(-0.069)$	$-6.473e^{-2}$–6.473×10^{-2}
Ni_4B_2	$B_5(0.080)$	$Ni_1(-0.040)$	$-5.190e^{-2}$–5.190×10^{-2}

Table 3 Atomic contributions to the orbit[a]

Symbol		FED^2_{HOMO}	$2FED^2_{HOMO}$	FED^2_{LUMO}	$2FED^2_{LUMO}$	$FED^2_{HOMO} + FED^2_{LUMO}$
NiB_2	B_1	0.2135	0.42706	0.2456	0.49124	0.4592
	B_2	0.2135	0.42706	0.2456	0.49124	0.4592
	Ni_3	0.5429	1.08582	0.4661	0.9322	1.0090
	H_4	0.0150	0.03004	0.0213	0.04266	0.0364
	H_5	0.0150	0.03004	0.0213	0.04266	0.0364
Ni_2B_2	B_1	0.2066	0.41322	0.0881	0.17628	0.2948
	B_2	0.2066	0.41316	0.0882	0.1763	0.2947
	Ni_3	0.2934	0.5868	0.4119	0.8237	0.7053
	Ni_4	0.2934	0.5868	0.4119	0.82372	0.7053
Ni_3B_2	B_1	0.1093	0.21866	0.0313	0.06258	0.1406
	B_2	0.1094	0.2187	0.0313	0.06258	0.1406
	Ni_3	0.1978	0.39568	0.4878	0.9755	0.6856
	Ni_4	0.2917	0.58348	0.2248	0.44968	0.5166
	Ni_5	0.2917	0.58348	0.2248	0.44968	0.5166
Ni_4B_2	Ni_1	0.1824	0.36484	0.2370	0.47394	0.4194
	Ni_2	0.1822	0.36444	0.2365	0.47304	0.4187
	Ni_3	0.1822	0.36444	0.2365	0.47304	0.4187
	Ni_4	0.1824	0.36484	0.2370	0.47394	0.4194
	B_5	0.1354	0.27072	0.0265	0.05302	0.1619
	B_6	0.1354	0.27072	0.0265	0.05302	0.1619

[a] FED^2 is the amount of atomic contribution to the orbital.

Gibbs free energy of the molecule gradually increased, and the structure of the Ni–B molecule tended to stabilize. Among the four molecules, among which the most stable structure was that for Ni_4B_2, NiB_2 had a weaker binding energy compared to Ni_4B_2, while Ni_2B_2 and Ni_3B_2 were in a sub-stable structure.

3.4.2.2 Optimization of the molecular structure of NiB_2, Ni_2B_2, Ni_3B_2, and Ni_4B_2. The optimized structures of NiB_2, Ni_2B_2, Ni_3B_2, and Ni_4B_2 were used to analyze the electrostatic potential spectrum. As demonstrated, the red region represents a negative electrostatic potential value, indicating that it is easier to give electrons and is more nucleophilic than the other regions. Conversely, the blue region represents a positive electrostatic potential and is more likely to give electrons being more electrophilic than the other regions.[57,58]

As can be seen in Fig. 9, the blue regions of the molecules NiB_2, Ni_2B_2, Ni_3B_2, and Ni_4B_2 reacted preferentially, and all four molecules had the same atoms with binding sites on the Ni atom. Table 2 shows that in the NiB_2 and Ni_2B_2 structures, the Ni atom was positively charged and the B atom was negatively charged. In the Ni_3B_2 structure, the Ni atom was two positive and one negative, while the B atom was positive. In the Ni_4B_2 structure, the Ni atom was negatively charged and the B atom was positively charged. The Ni_3B_2 and Ni_3B_2 and Ni_4B_2 molecules were globally distributed with both the HOMO and LUMO, both of which were locally excited. The high agreement with the experimental results was indirectly consistent with the claim that Ni–B is an amorphous alloy.[59–63]

As can be seen from Table 3, FED^2 was the atomic contribution to the orbital. The attack object was guided by the $2FED^2_{HOMO}$ value; whereby, the larger the value, the more vulnerable the atomic position was to the attack of the electrophile. The Ni_3 atom in NiB_2, the Ni_3 and Ni_4 atoms in Ni_2B_2, and the Ni_4 and Ni_5 atoms in Ni_3B_2 made the largest contributions. The Ni_1 and Ni_4 atoms in Ni_4B_2 making the largest contributions were electrophilic reaction sites. The $FED^2_{HOMO} + FED^2_{LUMO}$ values predict the site of an attack by free radicals; whereby, the higher the value is, the more likely it is to be attacked. The Ni3 atoms in NiB_2, Ni_3 atoms in Ni_2B_2, Ni_3 atoms in Ni_3B_2, and Ni_1 and Ni_4 atoms in Ni_4B_2 contributed the most and were free radical reaction sites.[64–66]

4. Conclusion

The analysis tools used in the present study feature some general implications for other analysis methods for experimental data. Here, Ni–B–AC catalysts were prepared by an impregnation reduction, and showed good stability and catalytic activity during the hydrogenation of β-pinene. Analyzed for the first time, a detailed analysis of the data of β-pinene hydrogenation single-factors was carried out using hierarchical analysis, which was highly consistent with the experimental results. The factors influence the catalyst stability, the selectivity and conversion of pinene, and the catalyst availability for industrial production. The analysis ideas presented in this study are also instructive for the further design and development of amorphous catalysts in the direction of nickel-based hydrogenation, but need to be further assessed for the preparation of such catalysts.

Conflicts of interest

There are no conflicts to declare.

Acknowledgements

The authors wish to acknowledge the support of the Analysis and Testing Foundation of Kunming University of Science and Technology. The authors thank Dr Jiang for her assistance in this matter.

References

1 P. Wu, Y. Dai, T. Du, X. Chen, s. Zhao, Y. Guo and W. Fang, The Pyrolysis Kinetics and Heat Exchange Performance of Biomass Hydrocarbon Pinane, *Fuel*, 2022, **317**, 123453.

2 P. Wu, L. Zhang, S. Zhao and C. Wang, Density and Viscosity of the Ternary System Pinane + N-Dodecane + Methyl Laurate and Corresponding Binary Systems at $T=293.15$–333.15 K, *J. Chem. Eng. Data*, 2021, **66**(7), 2706–2716.

3 X. He, A. J. Barthel and S. H. Kim, Tribochemical Synthesis of Nano-Lubricant Films from Adsorbed Molecules at Sliding Solid Interface: Tribo-Polymers from α-Pinene, Pinane, and N-Decane, *Surf. Sci.*, 2016, **648**, 352–359.

4 A. K. Jeevanantham, D. Madhusudan Reddy, N. Goyal, D. Bansal, G. Kumar, A. Kumar, K. Nanthagopal and B. Ashok, Experimental Study on the Effect of Cetane Improver with Turpentine Oil on Ci Engine Characteristics, *Fuel*, 2020, **262**, 116551.

5 M. Raji; T. M. Le; A. Csámpai; V. Nagy; I. Zupkó and Z. Szakonyi, *Stereoselective Synthesis and Applications of Pinane-Based Chiral 1,4-Amino Alcohol Derivatives*, Synthesis, 2022.

6 L. Du, X. Yang, T. Zeng and Z. Chen, Synthesis and Characterization of Pinane-Base End Hydroxy Polyethers, *Polym. Mater.: Sci. Eng.*, 2013, **29**(11), 10–14.

7 D. Hobuß, J. Hasenjäger, B. Driessen-Hölscher, A. Baro, K. V. Axenov, S. Laschat and W. Frey, Novel α-Pinene-Derived Mono- and Bisphosphinite Ligands: Synthesis and Application in Catalytic Hydrogenation, *Inorg. Chim. Acta*, 2011, **374**(1), 94–103.

8 P. Liu, X. Liu, T. Saburi, S. Kubota, P. Huang and Y. Wada, Thermal Stability and Oxidation Characteristics of α-Pinene, β-Pinene and α-Pinene/β-Pinene Mixture, *RSC Adv.*, 2021, **11**(33), 20529–20540.

9 J. E. Sánchez-Velandia, E. Pájaro, A. L. Villa and F. Martínez-O, Selective Synthesis of Camphene from Isomerization of α- and β-Pinene over Heterogeneous Catalysts, *Microporous Mesoporous Mater.*, 2021, **324**, 111273.

10 S. Tanielyan, N. Biunno, R. Bhagat and R. Augustine, Anchored Wilkinson Catalyst: Hydrogenation of β-Pinene, *Top. Catal.*, 2014, **57**(17), 1564–1569.

11 L. Xie, X. Wang, F. Yu, B. Yuan and C. Xie, Preparation of Cis-Pinane *Via* α-Pinene Hydrogenation in Water by Using Ru Nanoparticles Immobilized in Functionalized Amphiphilic Mesoporous Silica, *RSC Adv.*, 2017, **7**(81), 51452–51459.

12 P. Huang, Q. Deng, L. Jiang, Y. Zhi, W. Yang, J. Huang, Y. Zheng, Y. Wang, S. Shan, T. Hu and H. Su, The Exploration of Sensitive Factors for the Selective Hydrogenation of α-Pinene over Recyclable Ni-B/KIT-6 Catalyst, *Catal. Lett.*, 2021, 1–14.

13 F. Yu, Y. Shi, F. Wu, B. Yuan, C. Xie and S. Yu, Aqueous-Phase Hydrogenation of A-Pinene Catalyzed by Ni-B Alloys Loaded on a Janus Amphiphilic Carbon@Silica Nanomaterial, *Ind. Crops Prod.*, 2022, **185**, 115140.

14 M. Tan, D. Wang, P. Ai, G. Liu, M. Wu, J. Zheng, G. Yang, Y. Yoneyama and N. Tsubaki, Enhancing Catalytic Performance of Activated Carbon Supported Rh Catalyst on Heterogeneous Hydroformylation of 1-Hexene *Via* Introducing Surface Oxygen-Containing Groups, *Appl. Catal., A*, 2016, **527**, 53–59.

15 E. Díaz, J. A. Casas, Á. F. Mohedano, L. Calvo, M. A. Gilarranz and J. J. Rodríguez, Kinetics of 4-Chlorophenol Hydrodechlorination with Alumina and Activated Carbon-Supported Pd and Rh Catalysts, *Ind. Eng. Chem. Res.*, 2009, **48**(7), 3351–3358.

16 S. Hou, J. Dong, Z. Zhu, L. Geng, Y. Ma and B. Zhao, Size-Tunable Ultrafine Pt Nanoparticles in Soluble Metal-Organic Cages: Displaying Highly Stereoselective Hydrogenation of α-Pinene, *Chem. Mater.*, 2020, **32**(16), 7063–7069.

17 H. Chen, D. He, Q. He, P. Jiang, G. Zhou and W. Fu, Selective Hydrogenation of P-Chloronitrobenzene over an Fe Promoted Pt, */AC Catalyst*, 2017, **7**, 29143.

18 Y. Xu, Y. Wang, C. Wu, H. Huang, Y. Zhang, J. Nan, H. Yu and Y. Zhao, Structure Effect of Activated Carbon in Ru/AC Catalysts for Hydrogenation of Phthalates, *Catal. Commun.*, 2019, **132**, 105825.

19 H. Zheng, Y. Xue, Y. Niu, X. Gao, Y. Wang, G. Ding and Y. Zhu, Synthesis of Methyl Glycolate *Via* Low-Temperature Hydrogenation of Dimethyl Oxalate over an Efficient and Stable Ru/Activated Carbon Catalyst, *J. Chem. Technol. Biotechnol.*, 2022, **97**(9), 2572–2580.

20 L. Zhang, Z. Xin, L. Gao, Z. Li, G. Wei and R. Mo, Ni-B Catalyst with Metal Modifiers for Partial Hydrogenation of

Fatty Acid, *Methyl Esters at Mild Conditions*, 2021, **133**(3), 1–12.

21 S. Song, L. Jiang, Y. Wang, Y. Zheng, Y. Bao and C. Shen, Preparation of Nano Ni-B/TiO_2-ZrO_2 Catalyst and Its Performance for Rosin Hydrogenation Ni-B/TiO_2-ZrO_2, *Fine Chemicals*, 2019, **36**(11), 2234–2242.

22 Z. Liu, Y. Li, X. Huang, J. Zuo, Z. Qin and C. Xu, Preparation and Characterization of Ni-B/Sio2sol Amorphous Catalyst and Its Catalytic Activity for Hydrogenation of Nitrobenzene, *Catal. Commun.*, 2016, **85**, 17–21.

23 G. Singh, L. Singh, J. Gahtori, R. K. Gupta and A. Bordoloi, Catalytic Hydrogenation of Furfural to Furfuryl Alcohol over Chromium-Free Catalyst: Enhanced Selectivity in the Presence of Solvent, *Mol. Catal.*, 2021, **500**, 111339.

24 Y. Liu, F. Fu, A. McCue, W. Jones, D. Rao, J. Feng, Y. He and D. Li, Adsorbate-Induced Structural Evolution of Pd Catalyst for Selective Hydrogenation of Acetylene, *ACS Catal.*, 2020, **10**(24), 15048–15059.

25 W. Wang, F. Zhang, Y. Zhang, L. Xu, Y. Pei and J. Niu, Liquid-Phase Hydrodechlorination of Trichloroethylene Driven by Nascent H_2 under an Open System: Hydrogenation Activity, Solvent Effect and Sulfur Poisoning, *J. Environ. Sci.*, 2021, **108**, 96–106.

26 J. Zhang, P. Liu, Y. Shi, C. Fu, Q. Lin, F. Liu and H. Pan, The Synergistic Effect of the Carbon Shell Pore Volume and Core Pd Size of Pd@Hollow@C-X for the Synthesis of H_2O_2, *New J. Chem.*, 2021, **45**(3), 1617–1625.

27 P. Yu, M. Fang, S. Ma, J. Cen and Z. Luo, Quantitative Evaluation of Coupling Effects of Pore Structures and Metal Loadings on Catalytic Hydrogenation of Tar Model Reactants over Sulfided Nimo/Γ-Al_2O_3 Catalysts: Role of Segmented Catalytic Active Phase Volumes, *Fuel Process. Technol.*, 2021, **224**, 107008.

28 J. Xu, A. Ibrahim, X. Hu, Y. Hong, Y. Su, H. Wang and J. Li, Preparation of Large Pore Volume Γ-Alumina and Its Performance as Catalyst Support in Phenol Hydroxylation, *Microporous Mesoporous Mater.*, 2016, **231**, 1–8.

29 J. H. Türkcan, H. Elçiçek and O. K. Özdemir, Optimization of Synthesis Parameters for Catalytic Performance of Ni–B Catalysts Using Response Surface Methodology, *Int. J. Hydrogen Energy*, 2021, **46**(11), 7903–7911.

30 D. Lim, G. Özkan and G. Özkan, Ni–B and Zr–Ni–B in-Situ Catalytic Performance for Hydrogen Generation from Sodium Borohydride, Ammonia Borane and Their Mixtures, *Int. J. Hydrogen Energy*, 2022, **47**(5), 3396–3408.

31 A. M. Dmitrachkov, I. K. Ren and A. V. Nartova, N–Doping of Alumina Thin Film Support to Improve the Thermal Stability of Catalysts: Preparation and Investigation, *Appl. Surf. Sci.*, 2021, **38**, 107383.

32 Y. Zhang, *Research on the Stability of Catalysts Characterized by Tg-Dta and Icp, 4th International Conference on Environmental and Energy Engineering*, IC3E, IOP Publishing Ltd, Sanya, China, 2020.

33 M. Wang, D. He, M. Huang, X. Wang and P. Jiang, In Situ Growth of Ni-B Nanoparticles on Ni Foam: An Efficient 3d Integrated Anode for Enzyme-Free Glucose Detection, *J. Alloys Compd.*, 2019, **786**, 530–536.

34 F. Yu, Y. Shi, F. Wu, B. Yuan, C. Xie and S. Yu, Aqueous-Phase Hydrogenation of -Pinene Catalyzed by Ni-B Alloys Loaded on a Janus Amphiphilic Carbon@Silica Nanomaterial, *Ind. Crops Prod.*, 2022, **185**, 115140.

35 P. Huang, D. Pan, Q. Lai, L. Jiang, Y. Zheng, Y. Wang, Y. Zhi, S. Shan, T. Hu and Y. Su, The Exploration of Dominant Factors for the Hydrogenation of A-Pinene over Ni–P/APO-$_{11}$, *Catal. Lett.*, 2021, **151**, 2851–2863.

36 S. Gupta, N. Patel, R. Fernandes, R. Kadrekar, A. Dashora, A. K. Yadav, D. Bhattacharyya, S. N. Jha, A. Miotello and D. C. Kothari, Co-Ni-B Nanocatalyst for Efficient Hydrogen Evolution Reaction in Wide Ph Range, *Appl. Catal., B*, 2016, **192**, 126–133.

37 C. Yang, B. Xiang, L. Jiang, F. Zhang, C. Liu, Y. Wang, Y. Zheng, Z. Liu and P. He, Selective Hydrogenation of α-Pinene on a Nickel Supported Aluminophosphate Catalyst: Process Optimization and Reaction Kinetics, *Int. J. Chem. Kinet.*, 2021, **53**(3), 440–456.

38 K. Li, B. Lu, X. Wang, J. Du and X. Miao, Efficient and Highly Selective Reduction of α-Pinene by Span-80/$NiCl_2\cdot 6H_2O$/Methanol/$NaBH_4$, *Chem. Ind. Eng. Prog.*, 2020, **39**(12), 5119–5124.

39 X. Guo, J. Duan, C. Li, Z. Zhang and W. Wang, Modified Bamboo-Based Activated Carbon as the Catalyst Carrier for the Gas Phase Synthesis of Vinyl Acetate from Acetylene and Acetic Acid, *Int. J. Chem. React. Eng.*, 2021, **19**(4), 331–340.

40 X. Feng, S. Liu, Y. Li, R. Kong and J. He, Study of the Performance of Nitrogen-Doped Modified Activated Carbon as Catalyst Carrier for the Selective Catalytic Reduction of NO with NH_3 at Low Temperatures, *Aust. J. Chem.*, 2022, **75**(3), 197–205.

41 X. Gai, D. Yang, R. Tang, M. Luo, P. Lu, C. Xing, R. Yang, Q. Ma and Y. Li, Preparation of Ni-Co/SiO_2 Catalyst by Ammonia Reflux Impregnation and Its CH_4-CO_2 Reforming Reaction Performance, *Fuel*, 2022, **316**, 123337.

42 J. Wang, Y. Sun, Y. Wu, X. Shen, R. Tu, E. Jiang and X. Xu, The Steam Reforming of Guaiacol for Hydrogen *Via* Ni/Al2o3: The Influence of Dispersion, *Int. J. Energy Res.*, 2020, **44**(4), 2754–2767.

43 D. Cheng, L. Zhang, Y. Zhu, H. Xia, N. Li, W. Song, H. Bai and H. Ma, Preparation and Properties of Electrodeposited Ni-B-Graphene Oxide Composite Coatings, *Materials*, 2022, **15**(6), 2287.

44 D. Lim, G. Ozkan and G. Ozkan, NiB and ZrNiB in-Situ Catalytic Performance for Hydrogen Generation from Sodium Borohydride, Ammonia Borane and Their Mixtures, *Int. J. Hydrogen Energy*, 2022, **47**(5), 3396–3408.

45 L. Zhang, Z. Xin, L. Gao, Z. Li, G. Wei and R. Mo, Ni-B Catalyst with Metal Modifiers for Partial Hydrogenation of Fatty Acid Methyl Esters at Mild Conditions, *J. Chem. Sci.*, 2021, **133**(3), 1–12.

46 A. Selka, N. A. Levesque, D. Foucher, O. Clarisse, F. Chemat and M. Touaibia, A Comparative Study of Solvent-Free and Highly Efficient Pinene Hydrogenation over Pd on Carbon, Alumina, and Silica Supports, *Org. Process Res. Dev.*, 2017, **21**(1), 60–64.

47 L. Xie, X. Wang, F. Yu, B. Yuan, C. Xie and S. Yu, Preparation Of: Cis-Pinane *Via* α-Pinene Hydrogenation in Water by Using Ru Nanoparticles Immobilized in Functionalized Amphiphilic Mesoporous Silica, *RSC Adv.*, 2017, **7**(81), 51452–51459.

48 H. Fan, T. Zheng, X. Liao, M. Sun, J. Fu, J. Zheng, N. Zhang and B. Chen, Stereoselective Hydrogenation of Platform Molecule α-Pinene under Solvent-Free Conditions, *ChemCatChem*, 2022, **14**, 5.

49 L. F. Villanueva-Jiménez, J. A. Vázquez-López, J. Yañez-Mendiola, V. Calzada-Ledesma and J. D. Anda-Suárez, Decision-Making System Based on a Fuzzy Hierarchical Analysis Process and an Artificial Neural Network for Flow Shop Machine Scheduling Model under Uncertainty, *IEEE Access*, 2021, **9**, 104059–104069.

50 A. Caggiano, F. Napolitano and R. Teti, Hierarchical Cluster Analysis for Pattern Recognition of Process Conditions in Die Sinking Edm Process Monitoring, *Procedia CIRP*, 2021, **99**, 514–519.

51 A. S. Abuzaid and H. S. Jahin, Combinations of Multivariate Statistical Analysis and Analytical Hierarchical Process for Indexing Surface Water Quality under Arid Conditions, *J. Contam. Hydrol.*, 2022, **248**, 104005.

52 A. Sharma and N. Rawal, The Selection of Wastewater Treatment Units Based on Analytical Hierarchical Process, *Recent Trends in Civil Engineering*, 2021, 1003–1019.

53 V. Gupta and M. K. Rohil, An Experimental Measurement of Contradictory Judgement Matrices in Ahp, *IEEE International Conference on Parallel*, Distributed and Grid Computing, 2nd edn, 2012, 527–532.

54 M. J. Frisch, G. W. Trucks, H. B. Schlegel, G. E. Scuseria, M. A. Robb,J. R. Cheeseman, G. Scalmani, V. Barone, G. A. Petersson, H. Nakatsuji, X. Li, M. Caricato, A. V. Marenich, J. Bloino, B. G. Janesko, R. Gomperts, B. Mennucci, H. P. Hratchian; J. V. Ortiz, A. F. Izmaylov, J. L. Sonnenberg, D. Williams Young, F. Ding, F. Lipparini, F. Egidi, J. Goings, B. Peng, A. Petrone, T. Henderson, D. Ranasinghe, V. G. Zakrzewski, J. Gao, N. Rega, G. Zheng, W. Liang, M. Hada, M. Ehara, K. Toyota, R. Fukuda, J. Hasegawa, M. Ishida, T. Nakajima, Y. Honda, O. Kitao, H. Nakai, T. Vreven, K. Throssell, J. A. Montgomery Jr., J. E. Peralta; F. Ogliaro M. J. Bearpark, J. J. Heyd, E. N. Brothers, K. N. Kudin, V. N. Staroverov, T. A. Keith, R. Kobayashi, J. Normand, K. Raghavachari, A. P. Rendell, J. C. Burant, S. S. Iyengar, J. Tomasi, M. Cossi, J. M. Millam, M. Klene, C. Adamo; R. Cammi, J. W. Ochterski, R. L. Martin, K. Morokuma, O. Farkas, J. B. Foresman and D. J. Fox, *Gaussian 16 Rev. C.01*, Wallingford, CT, 2016.

55 L. Tian and F. Chen, *Multiwfn: A Multifunctional Wavefunction Analyzer*, 2012, **33**(5), 580–592.

56 H. Y. Ammar, K. M. Eid and H. M. Badran, The Impact of an External Electric Field on Methanol Adsorption on $XB_{11}N_{12}$ (X=B, Co, Ni) Nano-Cages: A DFT and TD-DFT Study, *J. Phys. Chem. Solids*, 2021, **153**, 110033.

57 M. J. Alam, A. U. Khan, M. Alam and S. Ahmad, Spectroscopic (FT-IR, FT-Raman, 1H NMR and UV-vis) and DFT/TD-DFT Studies on Cholesteno [4,6-B,C]-2,5-Dihydro-1,5-Benzothiazepine, *J. Mol. Struct.*, 2019, **1178**, 570–582.

58 F. Bardak, C. Karaca, S. Bilgili, A. Atac, T. Mavis, A. M. Asiri, M. Karabacak and E. Kose, Conformational, Electronic, and Spectroscopic Characterization of Isophthalic Acid (Monomer and Dimer Structures) Experimentally and by DFT, *Spectrochim. Acta, Part A*, 2016, **165**, 33–46.

59 G. Chen, X. Zhu, R. Chen, Q. Liao, D. Ye, H. Feng, J. Liu, M. Liu and K. Wang, Structured Ni-B Amorphous Alloy Catalysts on Ni Foam for a Gas-Liquid-Solid Microreactor, *Catal.: Sci. Technol.*, 2020, **10**(6), 1933–1940.

60 Y. Kang, J. Henzie, H. Gu, J. Na, A. Fatehmulla, B. S. A. Shamsan, A. M. Aldhafiri, W. A. Farooq, Y. Bando, T. Asahi, B. Jiang, H. Li and Y. Yamauchi, Mesoporous Metal-metalloid Amorphous Alloys: The First Synthesis of Open 3D Mesoporous Ni-B Amorphous Alloy Spheres *Via* a Dual Chemical Reduction Method, *Small*, 2020, **16**(10), 1–7.

61 L. Xu, J. Peng, B. Meng, W. Li, B. Liu and H. Luo, Microscale Interface Synthesis of Ni-B Amorphous Nanoparticles from $NiSO_4$ by Sodium Borohydride Reduction in Microreactor, *High Temp. Mater. Processes*, 2016, **35**(8), 745–750.

62 F. Li, J. Liang, K. Wang, B. Cao, W. Zhu and H. Song, Hydrogenation of M-Chloronitrobenzene over Amorphous Ni-B/CNTs Catalysts: Promoting Effect of CNTs Confinement on the Catalytic Performance, *Can. J. Chem. Eng.*, 2017, **95**(10), 2012–2017.

63 Y. Ma, J. Dong, X. Yang, L. Niu, H. Zhang and G. Bai, Hydrogelator as Growth-Controlling Agent for Enhancing the Catalytic Activity of NiB Amorphous Alloy Catalyst, *Res. Chem. Intermed.*, 2018, **44**(12), 7861–7872.

64 Y. Kong, W. Xiong, H. Guo, W. Sun, Y. Du and Y. Zhou, Elastic and Thermodynamic Properties of the Ni-B System Studied by First-Principles Calculations and Experimental Measurements, *CALPHAD: Comput. Coupling Phase Diagrams Thermochem.*, 2010, **34**(2), 245–251.

65 M. Wang, J. Xie, K. Xue and L. Li, First-Principles Study of High-Pressure Structural Stability and Mechanical Properties of Ni_2B, *Comput. Mater. Sci.*, 2021, **194**, 110465.

66 I. Matsui, Y. Hisai, T. Uesugi, N. Omura, Y. Takigawa and K. Higashi, Suppression of the Thermal Embrittlement Induced by Sulfur Segregation to Grain Boundary in Ni-Based Electrodeposits, *Materialia*, 2019, **6**, 100312.